Neutron Diffraction Study of the Magnetic Properties of the Series of Perovskite-Type Compounds $[(1-x)\text{La}, x\text{Ca}]\text{MnO}_3$†

E. O. Wollan and W. C. Koehler
Oak Ridge National Laboratory, Oak Ridge, Tennessee

(Received May 9, 1955)

A study has been made of the magnetic properties of the series of perovskite-type compounds $[(1-x)\text{La}, x\text{Ca}]\text{MnO}_3$. The investigations have been made primarily by neutron diffraction methods, but x-ray diffraction measurements of lattice distortions and ferromagnetic saturation data are also included. This series of compounds exhibits ferromagnetic and antiferromagnetic properties which depend upon the relative trivalent and tetravalent manganese ion content. The samples are purely ferromagnetic over a relatively narrow range of composition ($x \sim 0.35$) and show simultaneous occurrence of ferromagnetic and antiferromagnetic phases in the ranges ($0 < x < 0.25$) and ($0.40 < x < 0.5$). Several types of antiferromagnetic structures at $x = 0$ and $x > 0.5$ have also been determined. The growth and mixing of the various phases have been followed over the whole composition range, the ferromagnetic and antiferromagnetic moment contributions to the coherent reflections have been determined, and Curie and Néel temperatures have been measured. The results have been organized into a scheme of structures and structure transitions which is in remarkable accord with Goodenough's predictions based on a theory of semicovalent exchange.

1. INTRODUCTION

A NEUTRON diffraction study has been made of the magnetic properties of the series of compounds $[x\text{Ca}, (1-x)\text{La}]\text{MnO}_3$, where x varies from zero to unity. For all values of the parameter x, these mixed oxides crystallize in various modifications of the perovskite structure. The ideal cube of a perovskite contains one molecule ABO_3, where A is a large ion, for example, La^{+3}, Nd^{+3}, Ca^{+2}, Sr^{+2}, Ba^{+2}, etc., located at the cube center; B is a small ion, Mn^{+3}, Co^{+3}, Ti^{+4}, Mn^{+4}, etc., situated at cube corners; and the three oxygen ions are at the midpoints of the cube edges. Many examples of the perovskite structure are known, only a few of which are perfectly cubic.

Jonker and Van Santen[1] have investigated the magnetic properties of a number of these perovskite-type compounds and have found that certain of the mixed oxides containing manganese or cobalt become ferromagnetic with Curie points ranging downward from about room temperature. Their measurements of saturation moments and Curie temperatures for the $(\text{La}, \text{Ca})\text{MnO}_3$ series to be considered here are reproduced together with associated data of this report in Figs. 12 and 15 of Secs. 9 and 10. Their saturation measurements represent the average ferromagnetic moments of the macroscopic specimens and the Curie points refer to the temperature of transition to the ferromagnetic state. Application of the neutron-diffraction technique has made it possible to obtain more detailed information about the magnetic properties of these compounds. The ferromagnetic properties have been more fully investigated and the system has been shown also to have a variety of antiferromagnetic structures.

2. PREPARATIONS AND CHEMICAL ANALYSIS OF THE SAMPLES

The manganite samples were prepared by the ceramic technique outlined by Jonker and Van Santen.[1] Oxides, carbonates or hydroxides of lanthanum, calcium and manganese in the desired proportions were mixed under ethanol in a ball mill, dried at 100°C, and prefired, usually in air, at 900°–1000°C.[2] The products resulting from prefiring were mixed again, pressed without binder into briquets and finally fired in a resistance furnace at temperatures ranging from 1100°C to 1400°C. A few preparations were also made from solutions of the nitrates of the metals.

Diffraction samples for many preparations were prepared in the usual way. The sintered briquets were broken up to a fine powder which was packed into a thin-walled aluminum or vanadium cylindrical cell. For preparations to be studied as a function of applied magnetic field, the briquets themselves were used.

The ionic composition of the preparations depends markedly upon the temperature and atmosphere of firing. This has been pointed out by Jonker and Van Santen and has also been observed in the present investigations. It has been possible, for example, to obtain $LaMnO_3$ preparations with tetravalent manganese concentrations ranging from 2% to 35%: the lowest concentration resulted from firing in nitrogen at 1400°C, the highest from firing in oxygen at 1100°C. Similarly, preparations of $CaMnO_3$ containing 71, 80, 91, and 97% tetravalent manganese were found after firing in oxygen at 1400°C, 1350°C, 1300°C, and 1075°C, respectively.

Because the magnetic properties of these mixed manganites are so strongly dependent on the percent Mn^{+4} content, this quantity has in all cases been de-

† A preliminary account of this work was presented at the Conference on Ferrimagnetism, U. S. Naval Ordnance Laboratory, Washington, D. C., October 11–12, 1954.

[1] G. H. Jonker and J. H. Van Santen, Physica **16**, 337 (1950); **19**, 120 (1953).

[2] We were aided in the preparation of starting materials by Mr. D. E. LaValle of the Analytical Chemistry Division.

TABLE I. Data summary.

Sample	No.	% Mn^{+4}	Temp.[a]	θ_c°K	θ_n°K	Structure type	μ_A^2	μ_F^2	$\bar{\mu}_{sat}$
$LaMnO_3$	12	2	*He, N, R, C, B*		100	*A*	15.12		
$LaMnO_3$	34	9	*H, R*			*A, B*	13.68	1.36	0.49
$LaMnO_3$	1	10	*He, N, R, W*		140	*A, B*	13.24		0.53
$LaMnO_3$	65	14	*He, N, R*			*A, B*	11.68	3.48[b]	0.92
$LaMnO_3$	73	18	*He, P, N, R*	170		*B, A*	3.44	8.92[c]	
$LaMnO_3$	3	20	*H, P, N, R, W*	170	160	*B, A*	2.08	11.44[d]	2.86
(0.89 La−0.11 Ca)MnO_3	61	29	*He, R*			*B*[e]			
(0.85 La−0.15 Ca)MnO_3	21	18	*N, R, W*	190		*B, A*	0.4	13.80	
(0.85 La−0.15 Ca)MnO_3	23	18	*N, R, W*	170		*B, A*	0.44	12.00	2.22
(0.75 La−0.25 Ca)MnO_3	28	32	*N, R, W*	180		*B*		12.60	3.48
(0.65 La−0.35 Ca)MnO_3	70	35	*P, N, R*	250		*B*		13.24[f]	
(0.6 La−0.4 Ca)MnO_3	4	44	*P, N, R, W*	260		*B*[g]		10.60	3.47
(0.5 La−0.5 Ca)MnO_3	16	49	*N, R*	260		*B*[g]		10.64	3.19
(0.5 La−0.5 Ca)MnO_3	41	51	*N, R, W*	250		*B*[g]		10.04	
(0.5 La−0.5 Ca)MnO_3	75	46	*He, N, R*			*B*[g,h]		9.96	
(0.5 La−0.5 Ca)MnO_3	66	58	*He, R*			*CE*			
(0.4 La−0.6 Ca)MnO_3	5	71	*H, P, N, R, W*		170	*CE*			
(0.25 La−0.75 Ca)MnO_3	18	78	*N, R, W*		165	*CE*			0.18
(0.20 La−0.80 Ca)MnO_3	74	80	*P, N, R*		165	*C*	8.92		
$CaMnO_3$	6	71	*H, N, R, W*		130	?			
$CaMnO_3$	20	80	*P, N, R*		130	*G*	3.40		
$CaMnO_3$	26	91	*N, R, W*		130	*G*	5.92		
$CaMnO_3$	32	97	*P, N, R*		110	*G*	7.04		

[a] The temperatures have been coded to save space: *He* =4.2°K, *H* =20.4°K, *P* =46°K, *N* =77°K, *R* =293°K, *C* =198°K, *B* =370°K, and *W* indicates that part of the pattern was observed at successively higher temperature values in the course of sample warmup.
[b] No field dependence for either type of reflection was observed at 5000 oersteds.
[c] At 4.2°K the 200 difference reflection was reduced to 0.41 of its no field value by 5000 oersteds.
[d] At 77°K the 200 difference reflection was reduced to 0.51 of its no field value by 5000 oersteds.
[e] At 77°K the 200 difference reflection was reduced to 0.40 of its no field value by 5000 oersteds.
[f] At 77°K the 200 difference reflection was reduced to zero by 5000 oersteds.
[g] Additional structure is observed at positions inside the 200 reflection.
[h] At 77°K the ferromagnetic reflections are reduced to zero by 5000 oersteds. The additional structure is field independent.

termined by chemical analysis.[3] In the analysis a portion of each preparation was dissolved in a known excess of standard ferrous sulfate solution and the excess ferrous iron was titrated with standard potassium permanganate solution to give the oxidizing power of the manganese in the sample. A second portion was dissolved in nitric acid and hydrogen peroxide and the manganese oxidized to permanganate by sodium bismuthate. A known amount of ferrous sulfate was introduced into the solution and the excess determined by standard permanganate to give total manganese. From the results of the two titrations the ionic concentration was computed. The ionic analyses are shown in Column 3 of Table I and they are believed to be reliable to within about 5%.

Some consideration has been given also to the effect of quenching on the properties of the manganite preparations. In those cases where powder diffraction samples were to be used, the samples were quenched in air from the firing temperatures. When the briquet was to be used, it was necessary to cool the specimen slowly in order to avoid excessive fracturing. This was usually done by turning off the furnace and continuing to pass the firing atmosphere over the sample during cooling. Within the errors of analysis and observation, no significant differences in samples of comparable composition prepared by the two methods were observed.

[3] These analyses were carried out by Mr. A. D. Horton of the Analytical Chemistry Division.

3. APPARATUS

In the early part of this study the magnetic neutron scattering measurements were made with the conventional neutron spectrometer fitted with a low temperature cryostat which allowed data to be taken down to liquid helium temperatures, 4.2°K.

For a more complete analysis of the magnetic scattering properties of these compounds it was, however, found necessary to obtain data with the sample maintained in a magnetic field at low temperatures. The incorporation of magnetic fields at low temperatures required the building of a new spectrometer which is shown here in Fig. 1. The magnet and cryostat assembly sits on the crystal table of a low sturdily built spectrometer. The counter (for which only a part of the support arm is shown) rotates around the center of the crystal table and the counter and crystal table are geared together in the usual 2 to 1 ratio. The flat character of this spectrometer was dictated by the small distance from the floor to the center of the neutron beam from the pile.

The lower part of the cryostat vacuum chamber consists of a brass box sealed around the pole pieces with *O*-rings. The front and rear faces are *O*-ring sealed aluminum cover plates with thin walled cylindrical sections for entrance and exit of the neutron beam from the crystal monochromator. The front cover plate is removed for sample mounting and alignment. The inner cryostat and sample assembly are held in accurate

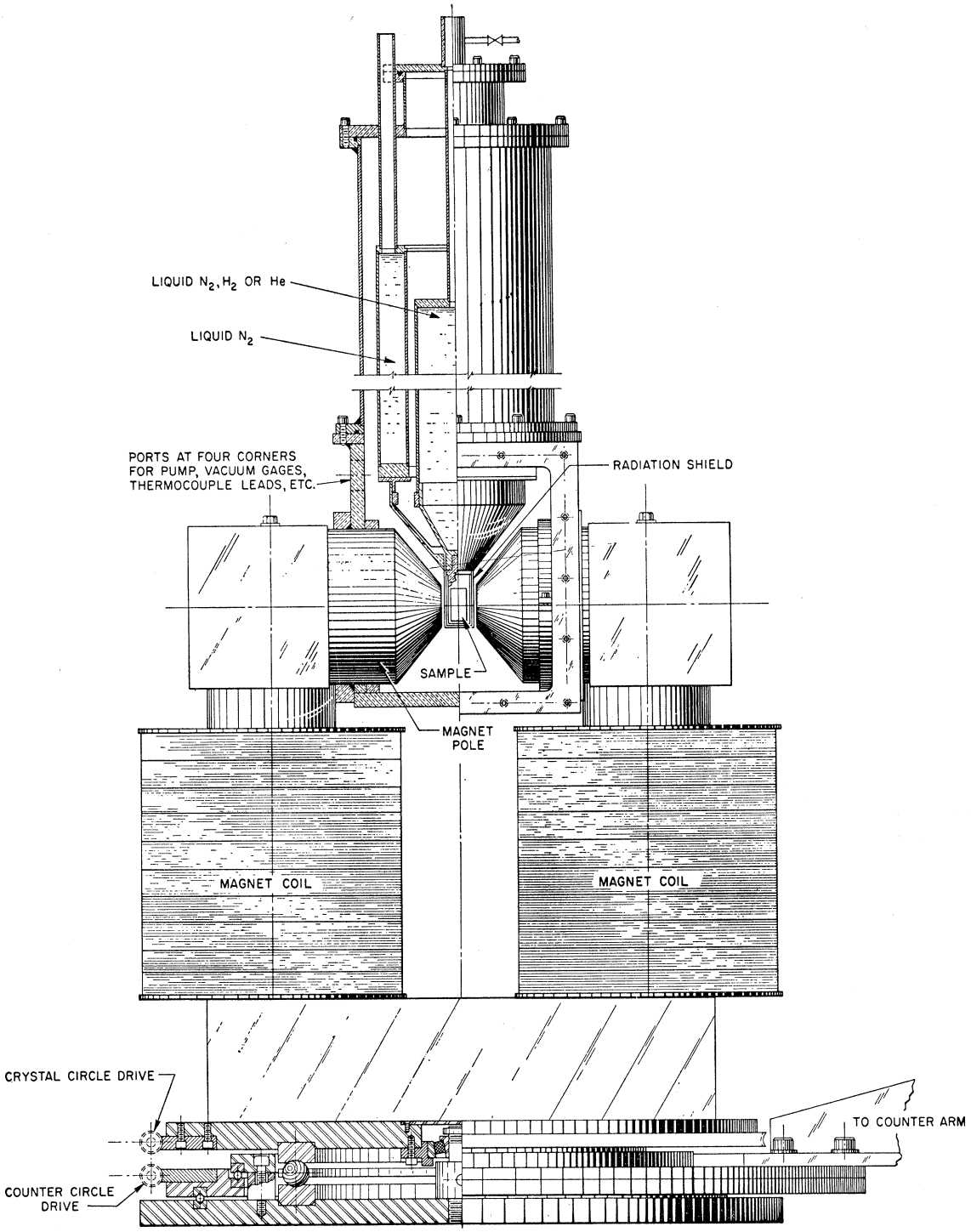

FIG. 1. Neutron spectrometer with cryostat and magnet.

alignment with the beam and the pole pieces by three nylon cords held taut by banjo type string tighteners anchored to the brass box.

The sample is cooled as previously by contact with the central dewar which for the lowest temperatures contained liquid helium. A thin-wall aluminum cylinder attached to this inner dewar and surrounding the sample constituted the inner radiation shield. This was in turn surrounded by a radiation shield in contact with the liquid nitrogen chamber. The samples were fre-

quently of cylindrical shape except when it was desired to make measurements with a magnetic field in which case the flat sintered plates shown in the figure were used.

For most of the runs the collimation of the scattered beam at the counter was effected by a boron carbide window but for some of the runs where greater resolution was required a Soller type slit was introduced in front of the counter.

During the course of this problem a new monitoring system was introduced in which the angular programing of the counter was determined by the monitor. The counter remained at each angular setting (intervals of 15 minutes of arc) until a prescribed number of monitor counts had been recorded and it was then automatically moved to the next setting.

The apparatus used in making ferromagnetic saturation measurements is described in Sec. 9.

4. DATA AND METHODS OF OBSERVATION

The character of the ferromagnetic data of Jonker and Van Santen suggested that antiferromagnetic ordering might be expected to develop in some samples at low temperatures. Neutron patterns were taken at room temperature and at one or more low temperatures at which antiferromagnetic structures as exhibited by super lattice lines were observed.

A sample neutron pattern taken at liquid nitrogen temperature (77°K) is shown in Fig. 2. This pattern was obtained with a sample of $LaMnO_3$ (identified in Table I as $LaMnO_3$ No. 1) which shows antiferromagnetic ordering at low temperatures (T_c=140°K). The cross-hatched reflections are superstructure lines arising from the antiferromagnetic ordering which has developed at 77°K. The other reflections in this case are due primarily to nuclear scattering.

In many cases it has been found advantageous in studying the magnetic scattering to determine the point by point difference curves between a run taken at room temperature and one taken at a low temperature well below the Curie or Néel point of the sample. In such a difference curve one eliminates effects such as the external background, multiple scattering, scattering by the sample holder and other parts of the equipment, in fact one eliminates all effects which are not dependent on the change in temperature of the sample. The difference curve does not, however, necessarily represent only the magnetic scattering effects because there are other temperature dependent phenomena. There is the Debye temperature effect on the nuclear reflections which for strong reflections can show up as residual difference peaks at the positions of these nuclear reflections. There are also possible crystallographic effects such as temperature dependent changes in the lattice parameters which cause shifts in the peak positions and thus effect the difference curves and there may be changes in atomic position parameters which produce changes in the peak intensities as a function of temperature as well as in the crystal symmetry. The extent of these temperature changes in the crystal which are extraneous to the magnetic effects determines in any case the usefulness of the temperature difference pattern in studying the details of the magnetic scattering. In representing the antiferromagnetic superstructure reflections, for example, it has not usually been found profitable to extend the difference curves into the region of the strong (111) nuclear reflection because effects of nonmagnetic origin in some cases become prominent in this region. The method of representing the data will thus depend on the properties of the particular sample being studied. The ferromagnetic effects can also be studied by the alternative approach of utilizing a magnetic field to turn off the ferromagnetic scattering. The application of this tech-

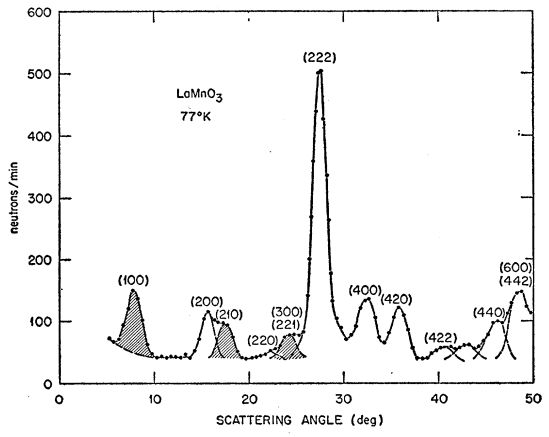

FIG. 2. Diffraction pattern for $LaMnO_3$ No. 1 at 77°K.

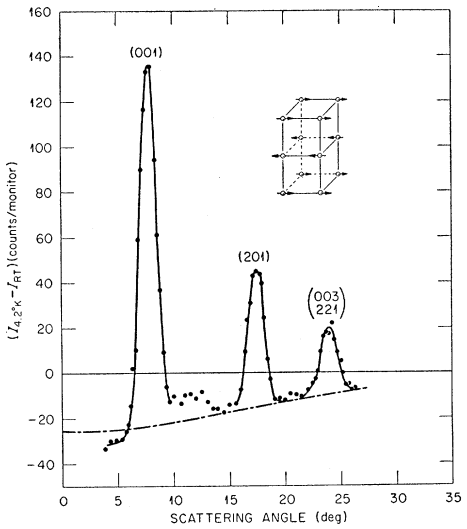

FIG. 3. Temperature difference pattern and antiferromagnetic structure (Type A) for $LaMnO_3$ No. 12.

nique is discussed in various connections in Secs. 7 and 8.

In the plot of a pattern involving the difference between a run taken at a temperature below the Curie or Néel point and a run taken at room temperature, where this is well above the critical point, the diffuse paramagnetic scattering features of the room temperature pattern will show up as a negative contribution in the difference pattern. There are features of this diffuse paramagnetic type scattering which are undoubtedly important to a complete understanding of the magnetic properties of these perovskite-type compounds but since they do not bear too directly on the magnetic structural aspects of these compounds, which is the primary subject of this paper, the details of the diffuse scattering features will be reserved for a future publication.

A summary of the samples studied and the data obtained for each is given in Table I. Discussions relative to these data are taken up in the following sections.

5. ANTIFERROMAGNETIC STRUCTURES OF $La^{+3}Mn^{+3}O_3$ AND $Ca^{+2}Mn^{+4}O_3$

$La^{+3}Mn^{+3}O_3$

A difference pattern ($I_{4.2°K}-I_{RT}$) for $LaMnO_3$ (Sample No. 12, Table I) obtained from data such as that shown in Fig. 2 together with a room temperature pattern is shown in Fig. 3.

The diffraction peaks[4] of this pattern are readily identified with an antiferromagnetic lattice consisting of layers of manganese ions coupled ferromagnetically (via intervening oxygen ions) in a given set of (001) planes but with alternate planes having opposite spin orientation, i.e., with antiferromagnetic coupling between planes. This structure is shown by the inset in Fig. 3, and as the A-type cell in Fig. 18. This arrangement calls for a unit magnetic cell doubled along one axis of the ideal elementary cubic cell. The indices identifying the reflections in the figure are nevertheless based on a cell doubled along all three axes in order to maintain uniformity in indexing later patterns which require increasing the cell in two or in all three directions. In addition to determining the ordering of the atomic moments one can determine also from the peak intensities for this cell whether the moments are directed approximately along the antiferromagnetic axis (taken as Z axis see Fig. 18) or in a plane perpendicular to this axis (X-Y plane). Since for the former case one would observe no intensity in the (001) reflection (see last column of Fig. 18 for predicted intensities) whereas experimentally this reflection is found to be strong, the moments must lie in or nearly in the X-Y plane. Although one might expect the moments to lie along one of the X or Y cube edges, this point cannot be ascertained in this case from powdered crystal measurements alone.

[4] The small peak near $2\theta=12°$ can be due to nuclear effects arising, for example, from shifts in oxygen parameters. This peak was not observed in patterns of $LaMnO_3$ of slightly higher Mn^{+4} content.

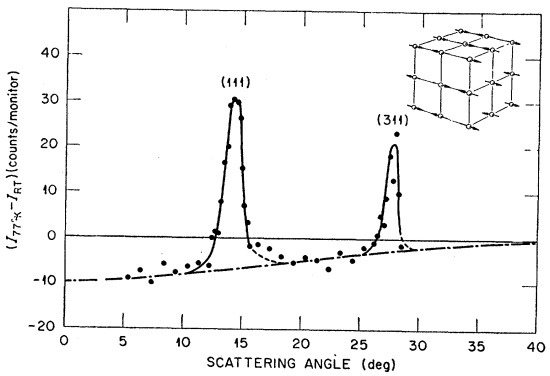

FIG. 4. Temperature difference pattern and antiferromagnetic structure (Type G) for $CaMnO_3$ No. 26.

The crystallographic properties of these compounds are taken up in detail in Sec. 11, but it is pertinent to note here that this sample departs from cubic symmetry in a manner consistent with the observed magnetic structure.

$Ca^{+2}Mn^{+4}O_3$

A difference pattern for $CaMnO_3$ No. 26 is shown in Fig. 4. It consists of two reflections which index as (111) and (311) on the basis of a cell doubled along the three edges of the simple chemical cell. This pattern is readily interpretable in terms of the structure given in the inset of Fig. 4, and identified as the G-type in Fig. 18 where the expected magnetic intensities are shown in the last column. Each Mn^{+4} ion is surrounded by six Mn^{+4} neighbors whose spins are antiparallel to the given ion. The structure can be thought of as consisting of two interpenetrating face centered lattices with opposite spin orientation.

6. OTHER ANTIFERROMAGNETIC STRUCTURES—EVIDENCE FOR ION ORDERING

In the composition range in which the Mn^{+4} content is greater than 50%, other antiferromagnetic type patterns are observed.

Figure 5 shows a temperature difference pattern for a sample [(0.20 La−0.80 Ca)MnO_3 No.74] with about 80% Mn^{+4}. The magnetic structure corresponding to this pattern is shown in the inset of Fig. 5 and as the C-type in Fig. 18. This cell calls for doubling of the simple cell in two directions but as before the lines in the pattern have been indexed for a cell doubled along all three axes. The intensities to be expected for this magnetic cell are shown in the last column of Fig. 18 for the two cases of spins along Z or in the X-Y plane. The intensities in the observed pattern correspond closely to case of spin parallel to the Z-axis.

In the C-type cell all atoms have two ferro- and four antiferromagnetic nearest neighbors whereas the reverse is true for the A-type cell.

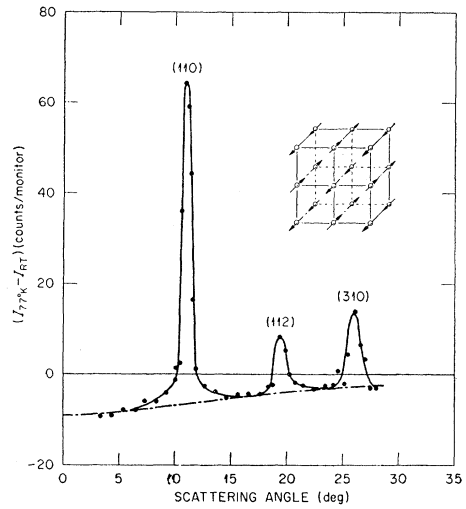

FIG. 5. Temperature difference pattern and antiferromagnetic structure (Type *C*) for (0.2 La−0.8 Ca)MnO_3 No. 74.

Up to this point antiferromagnetic patterns have been discussed for which the magnetic cells required doubling of the simple chemical cell along one, two, and three directions. For completeness in this respect one can add the ferromagnetic cell (discussed in the next section) for which the simple chemical cell and the magnetic cell are identical. These magnetic cells correspond to cases *A*, *B*, *C*, and *G* of Fig. 18. In each of these structures the ferro- and antiferromagnetic neighbor relations are the same for all the atoms in a given cell but the type of coupling and the relative number of ferro- and antiferromagnetic bonds varies with cell type.

We will consider next the pattern shown in Fig. 6 for a $CaMnO_3$ sample No. 6 having an Mn^{+4} content of about 70%. This pattern was obtained in the course of trying to prepare a pure $Ca^{+2}Mn^{+4}O_3$ sample. One notices here superstructure lines at the (100), (110), and (111) positions the simultaneous occurrence of which cannot be accounted for on the basis of any one of the previously encountered structures and also the intensities of these reflections do not correspond to the sum of the intensities from any incoherent mixtures of these structures. In view of this we were led to consider the other possible antiferromagnetic cells (*D*, *E* and *F*, Fig. 18) which require only doubling of the simple cell dimensions. These cells seem, *a priori*, no less acceptable than the previously observed cell types. Their magnetic neighbor and bond relations and the intensities in their diffraction patterns are also shown in Fig. 18.

The intensities in the pattern of Fig. 6 can be quite well accounted for as a mixture of magnetic phases of types *D* and *F* but at this stage we cannot be sure of the uniqueness of this interpretation. Further evidence for the incoherent mixing of magnetic phases will be seen to exist in connection with the composition range from greater than 0 to less than 50% Mn^{+4} content where both antiferromagnetic and ferromagnetic contributions to the pattern are simultaneously observed.

Further study of samples in this composition region ($x>0.5$) has, however, shown that some patterns cannot be accounted for by any of the cell types *A* to *G* or as incoherent mixtures of these magnetic structures. The first evidence for a more complicated magnetic structure came from a pattern which showed a broad peak at small angles when observed with the normal angular resolution. The difference pattern for sample (0.5 La−0.5 Ca)MnO_3 No. 66 taken with Soller slits to give better resolution is shown in Fig. 7.

The smallest unit cell upon which it is possible to index the observed magnetic reflections of this pattern is one which has $a=b=\sqrt{2}c$ where c is twice the Mn-Mn separation. The new a and b axes are thus face diagonals of the double cell (see inset in Fig. 18). The number of observed reflections which represents only a small fraction of those possible for this cell fall into two groups. In the one, single reflections (excluding permutations of indices) are observed with l odd, (101), (121), (301), etc., and in the other, contributions to a given peak can arise from superimposed even and odd l index reflections, (011) and (200), (311), and (202), etc. No single reflections with even l index are found nor are any reflections observed for planes of the form (001). Attempts to interpret the pattern with nonvanishing (200) and (202) reflections were not successful and hence the reflections in the latter group were ascribed to the (111) and (311) reflections only. On this basis all the observed reflections have l odd and this calls for a cell with all ions antiferromagnetically coupled in the c direction. The above considerations and a consideration of other absent reflections together with the fact that planes which contribute intensity cannot have a vanishing net spin lead to the arrangement of spins shown in the inset of Fig. 18.

It is interesting to observe that this spin arrangement can be developed by the coherent stacking of octants of the *C* and *E* type structures as shown by the octant

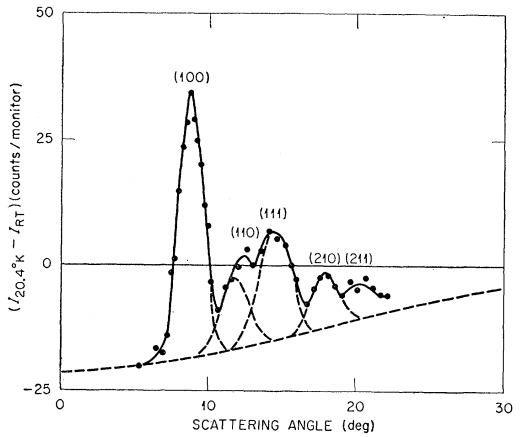

FIG. 6. Temperature difference pattern for $CaMnO_3$ No. 6.

labels in the structure diagram of Fig. 18. This stacking feature has led to the designation of this structure as the *C-E* type.

Although no other structure of this cell size has been observed, there are other possibilities two of which are represented by the *D-E* and *D-F* structures shown in the lower part of the figure. In the *C-E* type structure, which has been experimentally observed, the same simple ferro- and antiferromagnetic neighbor relations are present as in the case of the *C*-type alone, whereas the *D-E* and *D-F* cases are much more complicated in this respect.

So far the discussion of antiferromagnetic structures has been concerned only with the arrangement of the spins on the lattice sites and where possible with the orientation of the spin moments relative to the crystalline axes. In the case of the mixed oxides the magnetic structures may be associated with an ordering of the Mn^{+3} and Mn^{+4} ions on the lattice sites. In the *A*- and *G*-type structures this point did not enter. For the *C*-type structure the intensities are rather insensitive to ion ordering and no direct information on this point could be obtained from the data.

This is not true, however, for the *C-E* structure for which the predicted intensities are for some cases quite sensitive to the assumed distribution of the Mn^{+3} and Mn^{+4} ions on the lattice sites. Although this subject of ion ordering will be discussed later for all the mixed compounds in its relation to the nature of the magnetic coupling between ions, the experimental evidence for ion ordering will be presented here.

Before considering the effects of ion ordering it will be well to establish independently if possible the orientation of the spins relative to the crystalline axes. Calculations relative to both of these points are brought together in Table II. The first column gives the indices of the observed reflections based on the *C-E* type structure. The second column lists the values of q^2jF^2 deduced from the measured intensities in the pattern and succeeding columns list calculated values of this quantity. The first group of calculated values refers to a structure in which the Mn^{+3} and Mn^{+4} ions in equal proportions are distributed at random on the various lattice sites. Columns *a*, *b*, and *c* refer to the axis to which the spin vector has been assumed to be parallel.

TABLE II. Comparison of observed and calculated jF^2q^2 values for *C-E* type structure. Numbers in parentheses refer to percent Mn^{+3}—Mn^{+4}. *a*, *b*, *c* refer to axis along which spin is oriented.

		q^2jF^2 (10^{-24} cm^2/atom) Calculated					
		Disordered (50–50)			Ordered (50–50)	(42–58)	(44–56)
hkl	Observed	*a*	*b*	*c*	*a*	*a*	*a*
101	0.45	0.49	0.74	0.25	0.64	0.33	0.40
111	0.75	1.06	1.06	0.71	0.78	0.78	0.78
121	0.82	1.05	0.45	0.75	1.37	0.71	0.86
301	0.1	0.09	0.49	0.41	0.12	0.05	0.07
311	0.85	1.11	1.11	1.59	0.82	0.82	0.82

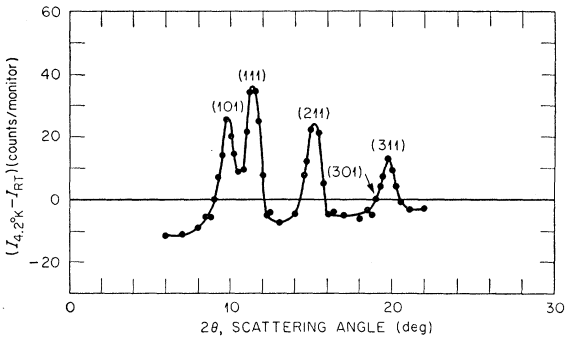

FIG. 7. Temperature difference pattern taken with Soller slits for (0.5 La—0.5 Ca)MnO_3 No. 66. *CE*-Type antiferromagnetic structure.

Although the agreement with the data is in no case very good, the low value predicted for the (301) reflection in the first column of this group suggests that the spins are oriented along the *a* axis. The fact that the calculations were made for a (50-50) ion composition whereas the sample analysis gave (42-58) has no effect on the relative values.

For the calculations involving ordering of the ions on lattice sites, two types of ordering have been considered.

One type results from simple phenomenological arguments about the types of indirect coupling between the magnetic ions in this system which are consistent with most of the data. The rules thus established which will be discussed more completely in Sec. 12 call for the indirect coupling in the region ($x>0.5$) to be ferromagnetic between unlike pairs and antiferromagnetic between like pairs of ions. The ion ordering obtained on the basis of these criteria puts Mn^{+3} and Mn^{+4} ions in positions for which the major intensity contributions are the same as for a disordered lattice. The ordering would lead to other nonvanishing reflections than those corresponding to the few observed lines in the pattern, but they would be too weak to have been observed.

The other type of ordering was suggested from a study of the pattern and it is of interest to observe that it fits well into a coupling scheme suggested by Goodenough (see following paper and Sec. 12 for further discussion on this point). This type of ion ordering is the one illustrated in the drawing of the *C-E* structure in Fig. 18.

For a pure structure of this type, the (101), (121), (301), etc., reflections would result from scattering by one kind of ion only and the (111), (311), etc., reflections would result from the other kind only. Unfortunately, the sample from which the pattern under consideration was obtained did not have a (50-50) ion composition, the results of the chemical analysis being (42-58). This fact makes it impossible to definitely verify this proposed type of ion ordering since additional assumptions must be made about the disposition of the excess Mn^{+4} ions.

Calculations relative to this type of ordering are

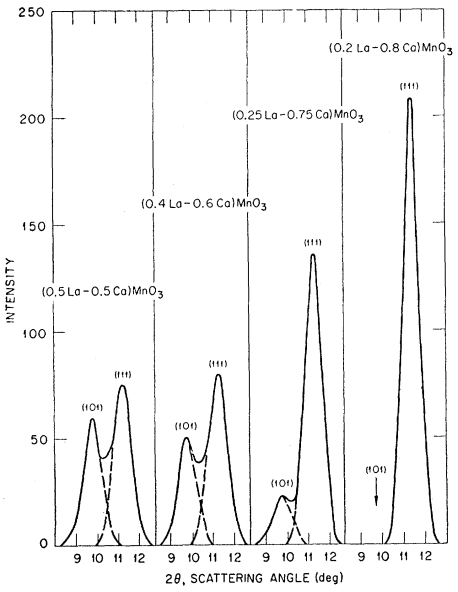

FIG. 8. First two antiferromagnetic reflections for four sample compositions showing the growth of a *C*-Type pattern (right) from the *CE*-Type (left).

given in the last three columns of Table II. The first column was calculated for the ideal composition. For the other two columns correction for composition was made on the assumption that the excess Mn^{+4} ions go at random but with opposite spin into sites occupied by Mn^{+3} ions in the ideal structure. The last column which agrees well with the experimental data was calculated for a slightly different composition than that given by the analysis but within the errors of the analysis.

The assumption that excess Mn^{+4} ions go into the Mn^{+3} sites with reversed spin is not completely arbitrary. If one examines the *C-E* type arrangement, one observes that one can obtain a *C* type structure by reversing half the spins of ions on the Mn^{+3} sites (as shown in Fig. 18) provided specific spins are so reversed. If this spin reversal is a result of the addition of Mn^{+4}, then one would expect that the *C* type structure should set in at a 75% Mn^{+4} concentration. Such a structure is in fact observed at 80% Mn^{+4}. It would seem reasonable to assume that in the early phases of this transformation the excess Mn^{+4} would go into the Mn^{+3} sites at random. A series of observations which suggested that this model for the transformation may be correct is shown in Fig. 8, where the first pair of reflections (101) and (111) are represented for various ion concentrations over the range 50%–80% Mn^{+4}. The intermediate compound (75 La−25 Ca)MnO_3 No. 18 is interesting in that it shows a much increased (111) reflection and a correspondingly decreased (101) reflection, and this indicates the approach to the *C*-type structure.

Before leaving the discussion of the *C-E* structure there is one point which should be mentioned. The discussion above relative to the deduction of the spin arrangement in this structure has assumed a single magnetic phase. Under the conditions that the structure is in fact defined by the unit cell described above and that there is antiferromagnetic coupling between adjacent layers, one can by exploring all of a reasonable number of possible spin arrangements conclude that the spin arrangement mentioned is unique. However, one may also put measurable intensities into and only into the positions observed in the pattern of Fig. 7 by an incoherent mixing of two phases: (1) the *C*-type which will reflect into the (111), (311), etc., position and (2) a cell of the same dimensions as the *C-E* type but built up of oriented octants of *E* type only (not illustrated) which may be called for the purpose of this discussion the *E-E* type and which puts intensity into the (101), (301), etc., positions. If one makes reasonable assumptions about the moment direction in the *E-E* arrangement and attempts to fit the observed intensities as an incoherent mixture of phases, one is led to inconsistencies which suggest the improbability of the incoherent arrangement. Further evidence from x-ray line splitting at low temperature which tends to support the *C-E* type arrangement is discussed in Sec. 12.

7. FERROMAGNETIC PATTERNS

One would expect from the saturation data of Fig. 12 and it is found from the neutron diffraction patterns that samples having a Mn^{+4} content in the neighborhood of 30% exhibit essentially pure ferromagnetic scattering with approximately the full predicted ferromagnetic moment per atom. Although the neutron patterns for sample compositions above and below this region also show ferromagnetic scattering, the situation becomes more complicated and these cases will be discussed in the following section.

Using the technique employed in the analysis of the antiferromagnetic patterns of plotting the difference between the low temperature and the room temperature data we obtained for sample (0.65 La−0.35 Ca)MnO_3 No. 70 the results shown in the lower half of Fig. 9. This pattern represents all the temperature dependent effects which occur between the two temperatures at which the patterns were taken, the greater part of which arises from magnetic scattering. The coherent peaks in this difference pattern fall at the positions of the nuclear reflections (the room temperature intensities of which are given above the pattern) as is to be expected for ferromagnetic scattering and the moments calculated from the two first peaks agree closely with the expected value. The third peak, however, is much too large to be due to magnetic scattering alone. There is, of course, the temperature effect for the strong nuclear peak at this position but on the basis of the *D-W* formula this would only correspond to that shown by the cross hatched portion for this and the succeeding peaks. One is thus led to conclude that minor changes

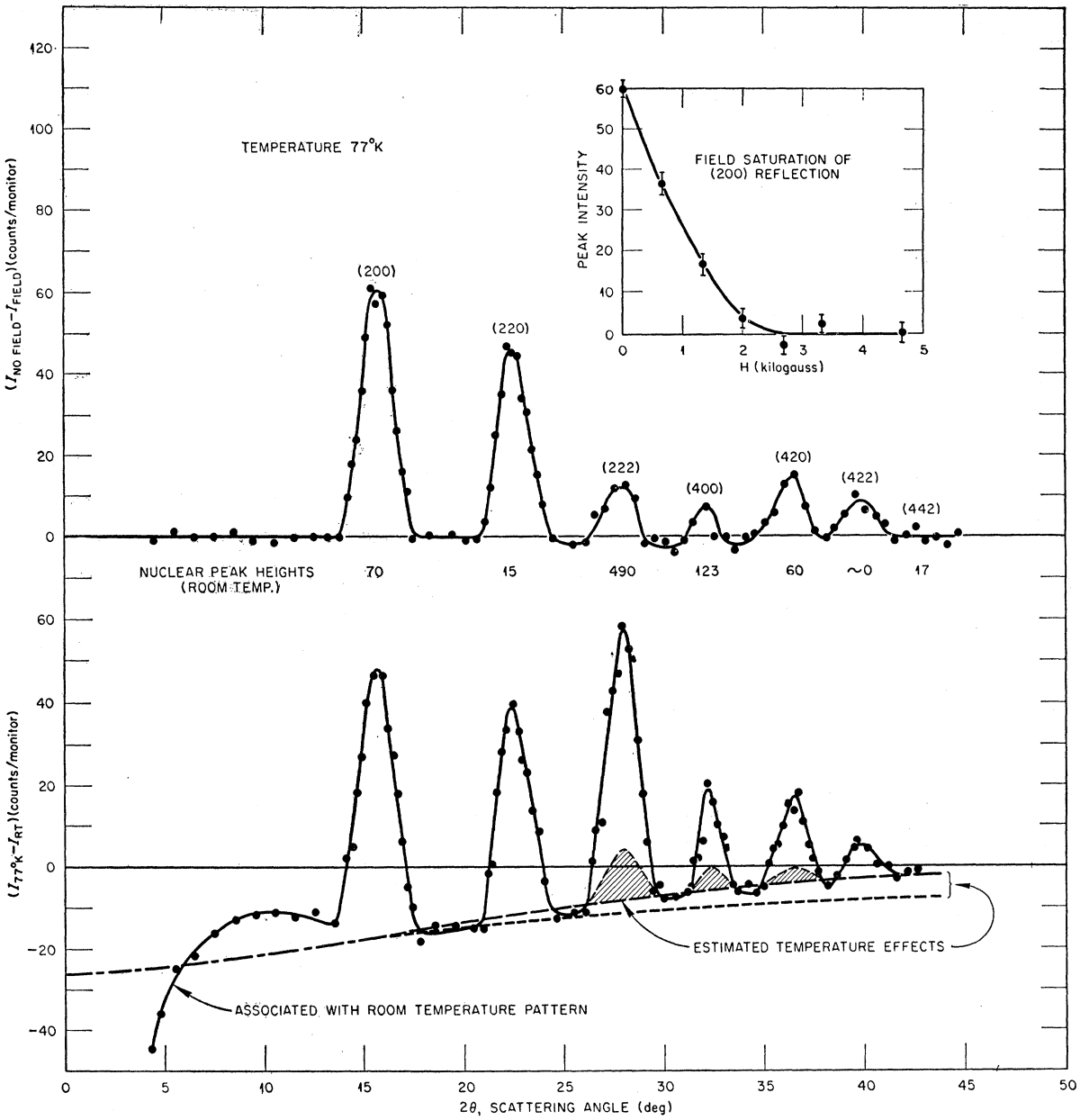

FIG. 9. Ferromagnetic patterns for [0.65 La—0.35 Ca]MnO_3 No. 70. Upper curve gives magnetic field difference pattern for maximum field in inset curve. Lower curve gives comparative data from temperature difference patterns.

with temperature of the atomic parameters are probably responsible for the anomalously large value of this peak.

The dashed curve represents the expected room temperature paramagnetic scattering. The anomalous behavior of the measured curve in the region from 4° to about 14° is undoubtedly due to a short range order effect in the room temperature pattern. Other patterns with a ferromagnetic component have shown a tendency to drop below the predicted curve at small angles and this effect has been identified with the room temperature data.

It must be concluded that the low temperature-room temperature difference pattern does not give an entirely reliable measure of the ferromagnetic scattering. In most cases the best approach to the study of the ferromagnetic scattering contribution is to use a magnetic field. Since the magnetic scattering goes to zero when the moments are all aligned parallel to the scattering vector the difference between measurements taken with zero field and with a field along the scattering vector of sufficient strength to align the domains gives a direct measure of the ferromagnetic scattering.

A difference pattern taken at liquid nitrogen temperature with and without magnetic field is shown in the upper part of Fig. 9 for the same sample used for the lower curve. It is seen from the figure that the (200) and (220) reflections have approximately the same integrated intensities in the upper and lower curves. This is also true of the corrected (400), (420), and (422) reflections but is definitely not the case for the (222) reflection. Although the background is field insensitive over much of the angular range, there is a definite indication that the difference curve drops below zero in the region from about 25° to 35°. The saturation curve for the magnetic scattering as measured on the first peak is shown in the inset.

A magnetic form factor can be obtained directly from this pattern but since this type of information is not especially pertinent to the main discussions of this paper, it will be reserved for future publication.

Although it appears from the above discussion that the use of a magnetic field is ideal for separating the nuclear and ferromagnetic scattering, it will be seen in the next section that in some cases the temperature difference method gives additional information.

8. MIXTURES OF FERRO- AND ANTIFERROMAGNETISM

In this section the nature of the magnetic scattering in the over-all range of Mn^{+4} content from near zero to about 50% will be considered. In the last section it was seen that for a sample having $x=0.35$ the scattering below the Curie temperature was essentially purely ferromagnetic in character as was to be expected since the saturation moment corresponded approximately to the theoretical value. In the region of $x<0.35$, however, the ferromagnetic saturation moment falls off rapidly from the maximum value and hence some modifications in the neutron patterns would be anticipated.

Difference patterns for a sample $LaMnO_3$ No. 73 -17.5% Mn^{+4} [5] in the region $x<0.35$ are reproduced here in Fig. 10. In the lower part of this figure the black circles represent $(I_{4.2°K}-I_{RT})$ taken with the usual geometry. The upper part of the figure shows $(I_{77°K}-I_{RT})$ taken with the same sample but with a Soller slit in front of the counter to give the improved resolution. The (200) and (220) reflections in these difference curves would be expected to arise essentially entirely from ferromagnetic scattering as illustrated by Fig. 9 for the purely ferromagnetic case. The cross hatched peaks (100) and (210), however, are at superstructure positions, in fact they correspond both in their positions and their relative intensities to those in the pattern of Fig. 3 corresponding to the A type of antiferromagnetic ordering. To account for this pattern having both antiferromagnetic and ferromagnetic scattering contributions one is first led to consider the possibility of crystallographic inhomogeneities in the sample. As a first crude experiment to test this point, a finely powdered sample was cooled below the Curie or Neél point and a small permanent magnet was held near the container. It was found that all the powder particles were attracted by the magnet and thus that any possible magnetic inhomogeneities in the sample were smaller than the particle size. Later x-ray studies by Yakel (see Sec. 11) showed the sample to possess a single crystallographic phase.

Since the sample is found to be crystallographically homogeneous one must account for the pattern of Fig. 10 on the basis (a) of some magnetic cell for which the moments in one direction do not compensate those in the other direction, a type of ferrimagnetism, or (b) of an incoherent mixture of regions or domains some of which are ferromagnetic and others antiferromagnetic with the A type structure; in addition there is, of course, the possibility that both of these situations may to some degree exist simultaneously. Although an analysis of the problem seems to favor hypothesis (b),

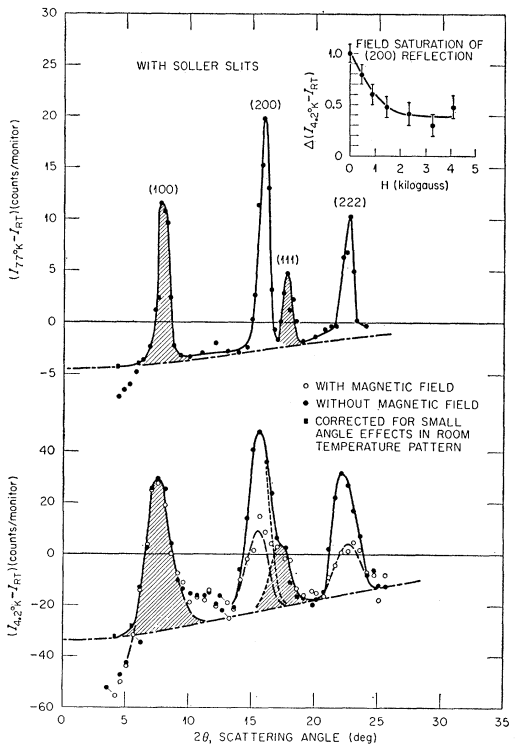

FIG. 10. Difference patterns for $LaMnO_3$ No. 73 with mixed ferro- and antiferromagnetic phases. Cross hatched lines represent antiferromagnetic contribution, others ferromagnetic. Upper curve taken with Soller slits, lower curve taken with usual resolution with and without magnetic field. Intensity *vs* field shown in inset.

[5] Although the ideal sample for this Mn^{+4} content should have the composition (0.83 La$-$0.17 Ca)MnO_3 it has been found that in this composition range the patterns are sensitive only to the Mn^{+4} content. For example, sample No. 23 shows essentially the same characteristics as sample No. 73. The latter sample is used here because it was made in the briquet form required for the measurements with a magnetic field.

at least as representing the major contributor, it was felt that a direct check of this point was important and it was primarily for this reason that the new spectrometer described in Sec. 2 was constructed. If ferromagnetism and antiferromagnetism appear in separate domains which are uncoupled or very weakly coupled, it would be expected that a magnetic field applied along the scattering vector would turn off only the ferromagnetic scattering peaks. If, however, the pattern were to be accounted for in terms of a homogeneously coupled system of some ferrimagnetic type the field would couple to the whole system and all the magnetic scattering could be turned off within the limits of field saturation.

The lower part of Fig. 10 shows the result of such a field study on this sample. The black circles, as we have mentioned, represent the difference curve ($I_{4.2°K}-I_{RT}$) with no field and the open circles represent the same pattern with a field of 4500 oersteds applied along the scattering vector. It is evident from these curves that the superlattice peaks are unaffected within experimental error by the field. It is also evident that with the available field the ferromagnetic type reflections are only partially obliterated. The saturation nature of the approach of the (200) peak height to its minimum value is shown as the inset in the upper part of Fig. 10. This type of curve was obtained only for a temperature of 77°K.

A discussion of the significance of the incomplete field sensitivity of the ferromagnetic type peaks in this and other patterns in the composition range will be discussed in Sec. 9 in connection with direct ferromagnetic saturation measurements. The fact that the magnetic measurements show the (200) and (220) ferromagnetic reflections to be field sensitive and the superstructure reflections (100) and (210) to be unaffected by the field is strong evidence in favor of accounting for the overall magnetic structure of samples in this composition range as consisting of an incoherent mixture of ferro- and antiferromagnetic regions or domains.

Although the data for only one sample in the composition range of Mn^{+4} less than 35% has been discussed here, several samples have been investigated to show the trend of the mixing in the range from the purely antiferromagnetic phase to the essentially purely ferromagnetic phase discussed in the last section. The other cases are tabulated in Table I and the nature of the overall results will be taken up in Sec. 13 in connection with the summary curve Fig. 19 of the ferro- and antiferromagnetic moments *versus* composition.

To complete the region involving ferromagnetic scattering there is shown in Fig. 11 a difference pattern for a sample (0.6 La−0.4 Ca)MnO_3 No. 4 with an Mn^{+4} content of 44%. This pattern shows primarily ferromagnetic scattering as represented by the main peaks but one sees also a small amount of antiferromagnetic contribution in the angular range 7 to 15 degrees and in the neighborhood of 20 degrees. Although this

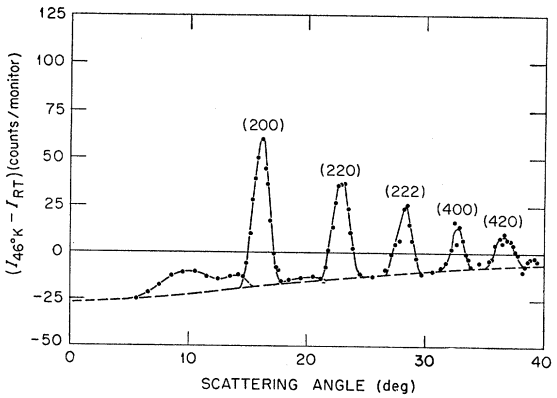

FIG. 11. Temperature difference pattern for (0.6 La−0.4 Ca)MnO_3 No. 4 for which there is some antiferromagnetic scattering.

scattering is too weak to permit identification with a definite magnetic structure, there is good reason to believe from comparisons with other patterns taken with the same and better resolution that this corresponds to the *C-E* type of antiferromagnetic structure. One thus has most likely also on the high side of the maximum in the ferromagnetic saturation *versus* composition curve a region of mixed ferro- and antiferromagnetic phases.

9. FERROMAGNETIC SATURATION MEASUREMENTS

The ferromagnetic properties of samples in the low range of Mn^{+4} content as determined from the neutron studies did not fit too well with the saturation moment data of Jonker and Van Santen and hence it was felt that direct measurements of the saturation moments on the samples used in this study would be valuable. Since a double cryostat surrounded at its lower end by an oil cooled solenoid capable of producing a field of 5000 oersteds constant over several inches was available in the laboratory,[6] the following simple method of making saturation magnetization measurements was used which tests indicated to be reliable at least to within a few percent. A small coil of 100 turns wound on a thin wall tube was located in the liquid helium cryostat near the center and with its axis parallel to the field of the solenoid. This tube projected through the top of the cryostat and another loosely fitting concentric tube was used to hold a sample approximately coaxial with the 100 turn coil. The powdered samples contained in cylindrical cells 2 in. long by $\frac{1}{4}$-in. diameter were held in the center of the coil until they had come to thermal equilibrium with the cooling liquid. The measurements were made by withdrawing the samples and reading the deflection of a ballistic galvanometer connected to the coil. The readings were standardized by comparison with the readings from a powdered Ni sample. For those samples for which these measurements were made, the results are tabulated in

[6] We are indebted to Dr. L. D. Roberts for the use of this equipment.

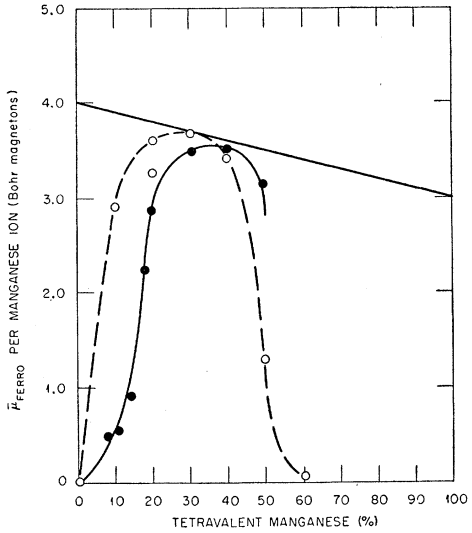

FIG. 12. Ferromagnetic saturation data *vs* composition. Open circles Jonker and Van Santen, solid circles present work.

the last column of Table I as the average moment per atom in Bohr magnetons. These data are shown also in Fig. 12 together with the corresponding data of Jonker and Van Santen. It is to be noted that our measurements are lower than those of Jonker and Van Santen in the region of low Mn^{+4} content and this point will come into evidence again later when a comparison is made with the corresponding neutron diffraction results.

An additional aspect of these measurements relates to the nature of the *B-H* curves. There would seem to be no question about temperature saturation since the measurements were made at liquid helium temperature. There is, however, a problem in some samples about field saturation. Those samples such as No. 70 which have a high moment are found to behave very normally reaching saturation at low fields. For the case of sample No. 65 with ~14% Mn^{+4} content (and for those of lower Mn^{+4} content) unusual *B-H* curve characteristics are observed as illustrated in Fig. 13. There seem here to be at least two types of magnetic behavior and it would appear also that saturation is not complete at 5000 oersteds. The peculiar character of this *B-H* curve has a bearing on the data to be discussed in Sec. 19 but the nature of the magnetic phenomenon involved has not been determined.

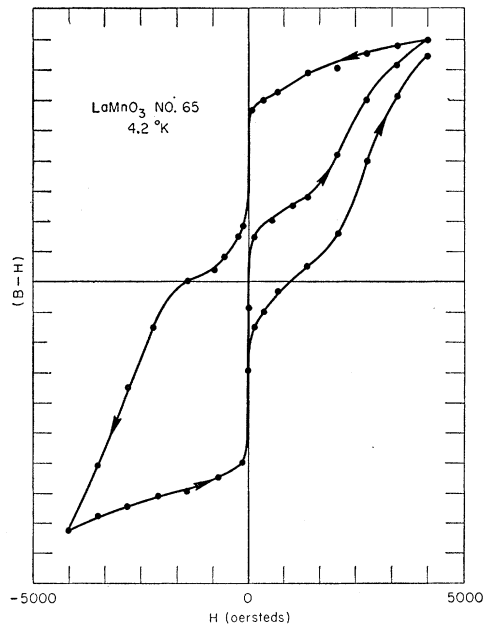

FIG. 13. *B-H* curve for $LaMnO_3$ No. 73.

10. THE CURIE OR NÉEL TEMPERATURE

Since the intensity of a coherent magnetic reflection in a neutron pattern depends upon the degree of temperature saturation of the magnetic lattice one can measure the temperature of transition to an ordered magnetic state by observing the temperature dependence of the intensity of a coherent magnetic reflection. Temperature-intensity curves were obtained for a number of the samples listed in Table I and a representative set of data is shown in Fig. 14. Intensity data were taken during a slow warmup from 77°K, and they were fitted by a Brillouin function, the intercept with the temperature axis of which was taken as the Néel temperature. The excess scattering at temperatures above the Neél point is probably due to short range magnetic ordering. This procedure was followed in cases for which 77°K was the lowest temperature at which patterns were obtained. In other cases, data at two or more fixed temperatures were extrapolated with a Brillouin function to give an estimate of the Néel or Curie point. In those instances where two phases are present, the transition temperature given in the table

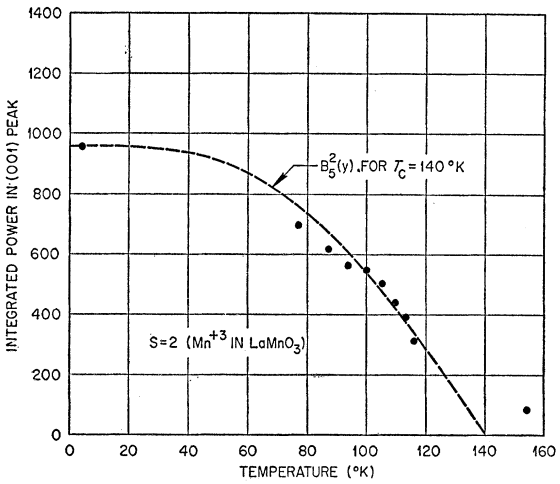

FIG. 14. Typical temperature saturation data with Brillouin curve.

refers to the dominant phase. In one case of a mixed phase sample ($LaMnO_3$ No. 3) the two transition temperatures appeared to be approximately equal. In another case ($LaMnO_3$ No. 73) there was an indication that the Neél temperature was some 30°K lower than the Curie temperature, but since the minor phase reflections are weak even at saturation, it is difficult to evaluate the minor phase transition points. The transition temperatures obtained by one or the other method outlined above are plotted in Fig. 15 in which are also shown the ferromagnetic Curie temperatures obtained by Jonker and Van Santen.

11. DETERMINATIONS OF APPARENT SYMMETRY AND LATTICE PARAMETERS

As a part of this investigation, x-ray diffraction data have been obtained by Yakel for all preparations at room temperature, and also at lower temperatures for a few selected samples. The room temperature results have already been described.[7] As Yakel has pointed out, the differences between the diffraction patterns obtained and those expected from an ideal perovskite structure consist of split reflections, and superlattice reflections which imply distortions of the lattice from cubic symmetry. Since, as shown by Megaw,[8] the number and relative intensities of the diffraction lines into which a given ideal reflection splits by distortion of the unit cube is characteristic of the symmetry of the distorted structure, it was possible to index the patterns and to determine the apparent symmetry of the preparations in most cases. In a few instances the splitting was so slight as to make the separate reflections almost indistinguishable, and in such cases only an average lattice parameter was measured.

The room temperature x-ray diffraction data are summarized in Fig. 16 in which are plotted the lattice parameters of our preparations against tetravalent manganese concentration. For tetravalent manganese concentrations up to about 25%, the splitting is characteristic of a monoclinic or orthorhombic symmetry, and this splitting decreases with increasing tetravalent manganese concentration. As represented in the figure, the apparent symmetry is taken as monoclinic, but since within experimental error the a_1 and a_3 axes of the monoclinic cell are equal, an orthorhombic cell with a_1 and a_3 axes equal to the diagonals of the rhombus formed by the monoclinic a_1 and a_3 axes may also be defined. Which of these correctly describes the symmetry of the unit cell cannot be decided from powder data alone. The splitting which is observed in the 0–25% concentration range seems to depend primarily upon the tetravalent manganese content of the preparation since mixed oxides and $LaMnO_3$ preparations with corresponding ion concentrations exhibit similar splittings. For the entire series of preparations except for the

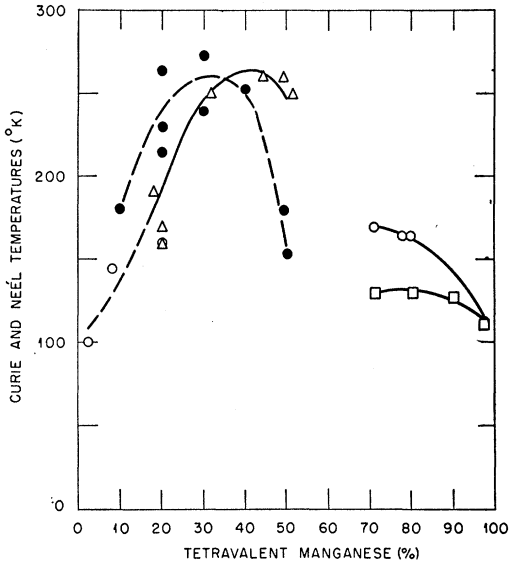

FIG. 15. Curie and Néel temperatures *vs* composition. Solid circles Jonker and Van Santen ferromagnetic saturation data, open triangles ferromagnetic neutron data, open circles and squares antiferromagnetic data, square referring to $CaMnO_3$ series.

$CaMnO_3$ samples with fairly high trivalent manganese concentration, the average lattice constant as defined by the approximate relation $\bar{a}=V^{\frac{1}{3}}$ (where V is the

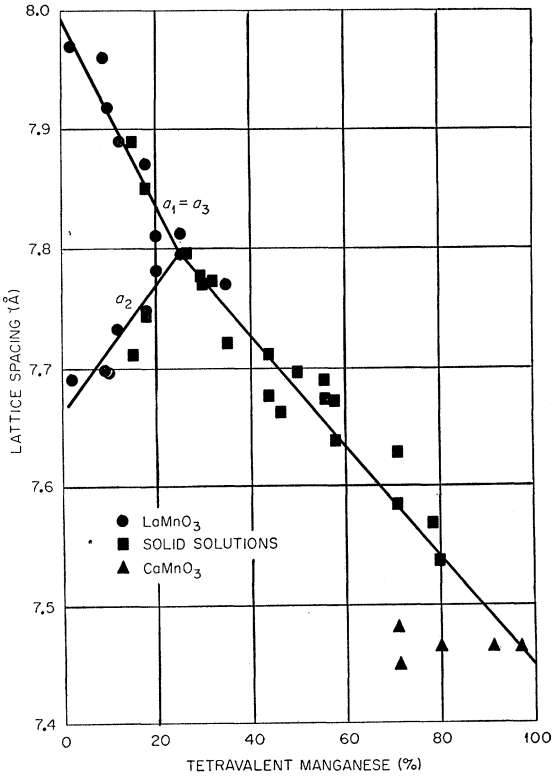

FIG. 16. Room temperature lattice constants from x-ray measurements. Yakel.

[7] H. L. Yakel, Acta Cryst. (to be published).
[8] H. D. Megaw, Proc. Phys. Soc. (London) **58**, 133 (1946).

TABLE III. Summary of x-ray diffraction data.

Sample	R.T. Mn^{+4} %	Apparent symmetry	Lattice parameters	T (°K)	Low temp. Remarks
$LaMnO_3$ No. 12	2	Monoclinic	$a_1=a_3=7.973$ A, $a_2=7.693$ A, $\beta=92°\ 7'$	80	No further splitting
$LaMnO_3$ No. 34	9	Monoclinic	$a_1=a_3=7.960$ A, $a_2=7.698$ A, $\beta=91°\ 52'$	93	Very slight additional splitting
$LaMnO_3$ No. 65	12	Monoclinic	$a_1=a_3=7.891$ A, $a_2=7.737$ A, $\beta=91°\ 9'$	80	No further splitting
$LaMnO_3$ No. 3	20	Monoclinic	$a_1=a_3=7.809$ A, $a_2=7.782$ A, $\beta=90°\ 12'$	93	No further splitting
(0.85 La−0.15 Ca)MnO_3 No. 21	18	Monoclinic	$a_1=a_3=7.848$ A, $a_2=7.734$ A, $\beta=90°\ 45'$	83	Very slight additional splitting
(0.5 La−0.5 Ca)MnO_3 No. 16	49	Cubic	$a_1=7.697$ A	93	No splitting
(0.5 La−0.5 Ca)MnO_3 No. 75	46	Unmeasurable splitting	$\bar{a}=7.662$ A	78	No further splitting
(0.5 La−0.5 Ca)MnO_3 No. 66	58	Monoclinic	$a_1=a_3=7.672$ A, $a_2=7.638$ A, $\beta=90°\ 12'$	78	Tetragonal $a_1=7.713$ A, $a_3=7.515$ A
(0.4 La−0.6 Ca)MnO_3 No. 5	71	Tetragonal	$a_1=7.628$ A, $a_3=7.584$ A	87	Tetragonal $a_1=7.668$ A, $a_3=7.508$ A
(0.25 La−0.75 Ca)MnO_3 No. 18	78	Cubic	$a_1=7.568$ A	81	Tetragonal $a_1=7.612$ A, $a_3=7.476$ A
(0.20 La−0.80 Ca)MnO_3 No. 74	80	Cubic	$a=7.539$ A	86	Tetragonal $a_1=7.466$ A, $a_3=7.636$ A
$CaMnO_3$ No. 6	71	Monoclinic	$a_1=a_3=7.481$ A, $a_2=7.449$ A, $\beta=91°\ 7'$	93	No further splitting
$CaMnO_3$ No. 26	91	Cubic	$a_1=7.465$ A	80	No splitting

volume of the unit cell) follows a straight line with negative slope and displays the expected decrease in cell size due to the smaller ionic radius of tetravalent manganese. This relation for the average spacing also holds for the compounds in the 0–25% region but it is to be noted that the a_2 axis increases, the a_1 and a_3 axes decrease over this region. It is therefore indicated that the $LaMnO_3$ preparations are characterized by cation defects rather than by interstitial anions but that the defects do not play a very important role with regard to the interatomic distances.

Some observations were also made which suggest that these defects adjust themselves to the atmosphere and temperature of firing and are formed reversibly. For instance a preparation of $LaMnO_3$ was fired at 1400°C in an atmosphere containing 1% O_2-99% N_2 and the resulting preparation showed a large room temperature splitting with $a_1=a_3=7.950$ A, $a_2=7.700$ A. This same preparation was then refired in oxygen at 1200°C and diffraction patterns showed a very much decreased splitting; $a_1=a_3=7.812$, $a_2=7.794$. After firing again in nitrogen at 1400°C, the large splitting corresponding to $a_1=a_3=7.960$ A, $a_2=7.698$ A was again observed.

Some preparations of $CaMnO_3$ with less than 100% tetravalent manganese were obtained in the course of preparing a pure sample. One of these was apparently monoclinic, the other three cubic but in every case the average lattice constant was approximately the same. Since the presence of trivalent manganese would be expected to increase the average lattice spacing, these results suggest the presence of anion defects which would offset the expected expansion of the cell.

For intermediate ion concentrations there are observed at room temperature apparent symmetries which are cubic, tetragonal, and monoclinic or orthorhombic. Some of the preparations are described in Table III, and a complete tabulation is given by Yakel.[7]

Crystallographic changes which are associated with magnetic ordering, particularly with the development of antiferromagnetic structures have been observed for a large number of compounds.[9] Since the magnetic ordering which develops in the manganites does so at low temperatures, a number of preparations have been examined by x-ray diffraction methods at temperatures slightly above 77°K. The results of this study are shown in Table III.[10] For specimens in the 0–50% concentration range, very little further splitting was observed. In the region of 55%–85% except for $CaMnO_3$ No. 6 an additional splitting of appreciable magnitude was detected. Of the four samples listed which show this effect, the first three exhibit the magnetic structure which we have designated as the *C-E* type, the fourth one belongs to the *C* type. In each case the splitting pattern suggests a tetragonal cell but in the first three instances the tetragonal axis decreases whereas for the *C* type magnetic structure the tetragonal axis increases over the room temperature value. The transition from the room temperature to the low temperature diffraction patterns for these substances is not sharp but extends over a large temperature range. A typical curve showing the variation of lattice parameter with temperature is shown in Fig. 17. One sees from this curve that the splitting increases with decreasing temperature and apparently levels off to a maximum at about 150°K. The Neél temperature for this sample as determined from the neutron data is approximately 165°K.

It is indicated that the crystallographic distortion which occurs, does so at a temperature considerably above the Neél point and it has been suggested by Goodenough[11] that the crystallographic distortion is due to an ordering of covalent bonds in such a way as to minimize the elastic distortions while permitting the formation of the optimum number of covalent bonds. In pursuing these arguments Goodenough has been led to infer from the c/a ratios (<1 for *C-E*; >1 for *C*) a system of ionic ordering which is in agreement with the neutron diffraction observations and thus lends support to our assignment of sample 18 to the *C-E* structure type.

The room temperature neutron patterns, even for the concentration range for which the apparent symmetry was found by x-ray measurements to be cubic, all

[9] See for instance the review article by Nagamiya, Yosida, and Kudo, Advances in Physics 4, 2 (1955).

[10] H. L. Yakel (private communication).

[11] John B. Goodenough, following paper, Phys. Rev. **100**, 564 (1955).

showed evidences of distortion from the simple cubic perovskite structure. This evidence consists of (1) the lack of agreement between the neutron intensities observed and those calculated on the basis of the simple cubic perovskite structure and (2) in some cases weak but measurable lines at positions which require a doubling of the simple cell. Such effects have been noted also by Roth in a preparation of (La, Ba)MnO_3.[12]

The observed powder intensities can be better correlated if the oxygen ions are displaced from the special positions of the ideal perovskite cell, for instance, if the oxygen tetrahedra are rigidly rotated in the manner proposed by Naray-Szabo in the $CaTiO_3$ structure.[13] Other conceivable distortions of the oxygen ion system all tend to improve the intensity agreement. Therefore, powder data alone do not seem sufficient for a definite decision as to the structure distortions and a more complete study must be carried out with single crystals.

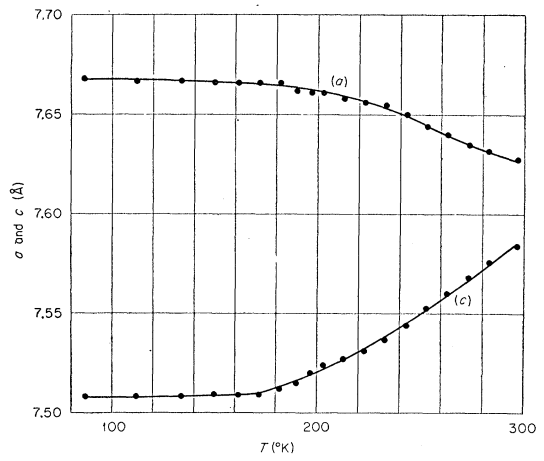

FIG. 17. Temperature dependence of lattice constants for a typical *CE*-Type sample. Lattice constants are twice those of the simple cubic cell.

12. SUGGESTED DISTRIBUTION AND COUPLING OF Mn^{+3} AND Mn^{+4} IONS IN VARIOUS MAGNETIC STRUCTURES

The correlation of the observed magnetic structures of this series of compounds with Mn^{+3} and Mn^{+4} ion concentration should give information about the type and strength of coupling between these ions. From the over-all structural aspects of the system one is led to the conclusion that the exchange coupling in general is (a) ferromagnetic between Mn^{+3} and Mn^{+4} ions (b) antiferromagnetic between Mn^{+4} ions and (c) either ferromagnetic or antiferromagnetic between Mn^{+3} ions, the type being related to the separation between ions.

It would also seem reasonable to suppose that long range ordering of the magnetic moments would be accompanied by some degree of ordering of Mn^{+3} and Mn^{+4} ions on correspondingly appropriate lattice sites. This ordering requires only that an electron be free to shift readily from one ion to another.

On the basis of these hypotheses a system of ordered magnetic structures can be developed as shown by the single octant entries in Columns 3 to 7 of Fig. 18. Pertinent points relative to these proposed structures will be considered in the order in which they appear. For convenience they will sometimes be labeled with the letter in the first column and the Mn^{+3}, Mn^{+4} content listed at the top of Columns 3 to 7. It will be seen in the following that one or more of the set of preliminary conclusions above must be relaxed for certain composition ranges.

Pure Mn^{+3} Phase ($x=0$)

In the ideal $LaMnO_3$ phase all manganese ions are trivalent and one must look to a crystallographic or bond character origin for the fact that there is ferromagnetic coupling along two axes and antiferromagnetic coupling along the third axis. There is indeed a striking correlation between the magnetic structure and the nearly tetragonal character of the crystal structure for $x=0$, the lattice parameters of which are shown in Fig. 16 for room temperature and which are not much altered for temperatures below the Neél point. The magnetic and crystal structure properties of this phase are both well accounted for by Goodenough's theory of bonding for these compounds. He associates with the Mn^{+3} ions four-lobed planar hybrid orbitals which can thus overlap the p orbitals of only four of the six oxygen neighbors. His proposal of an ordered system of such orbitals as represented schematically by the arrow heads in the A-8-0 entry in Fig. 18 will thus lead to the observed crystal symmetry if, as is to be expected, overlap on both sides of an intervening oxygen ion leads to a shorter Mn-O-Mn distance. His theory also makes overlap on both sides of an intervening oxygen ion the condition for antiferromagnetic coupling and hence this will correspond to the unique a_3 axis. From the x-ray measurements it may thus also be concluded that the Mn^{+3}-O-Mn^{+3} coupling will be antiferromagnetic when the separation of two Mn^{+3} ions is not much greater than 3.8 A.

Ferromagnetic Region ($0<x<0.5$)

With a relatively strong ferromagnetic coupling for Mn^{+3}-O-Mn^{+4} one is led to predict a stable ferromagnetic cell B-6-2 for a 25% Mn^{+4} content as shown in Column 4, Fig. 18. The presence of two Mn^{+4} ions per unit cell would then be sufficient to stabilize the ferromagnetic phase. With increasing Mn^{+4} content one would expect, if the ferromagnetic Mn^{+3}-O-Mn^{+4} exchange is dominant, the development of a structure B-4-4 in which every Mn^{+3} ion has six Mn^{+4} nearest neighbors. The behavior of the moments in the mixed

[12] Walter L. Roth, Pittsburgh Diffraction Conference, November, 1954 (unpublished).
[13] S. Naray-Szabo, Naturwiss. **31**, 202 (1943).

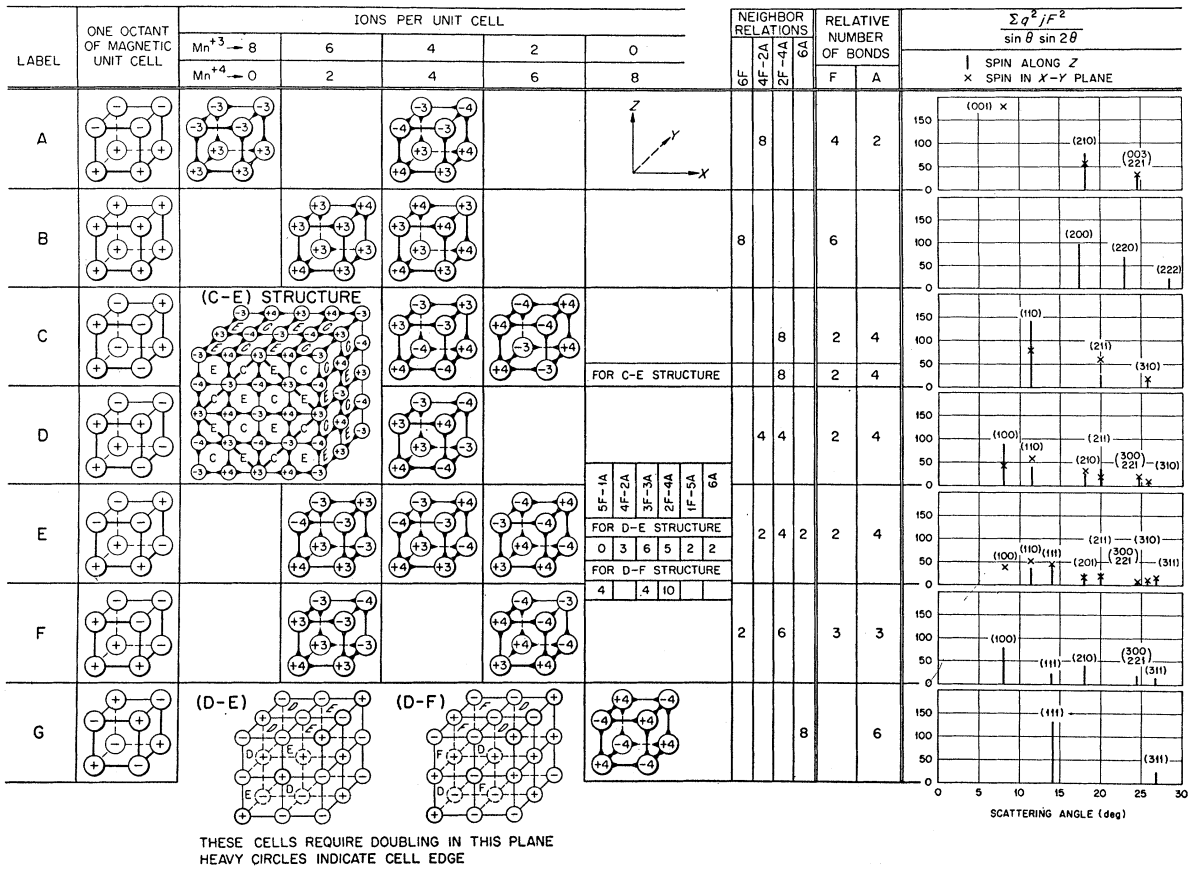

FIG. 18. Scheme of magnetic structures and related information. *A*, *B*, *C*, *G*, and (*C-E*) definitely observed and some evidence for *D* and *F*. Ion ordering schemes represent arrangements consistent with certain coupling criteria. Arrowheads are a schematic representation of Goodenough's semicovalent exchange coupling.

phase region ($0.1<x<0.25$) discussed in Sec. 13 indicates that there is a tendency for the Mn^{+4} ions to cluster and hence some tendency toward ordering of the type suggested by *B*-6-2.

Conversely, in the region ($0.25<x<0.35$) where the observed ferromagnetic moment is nearly equal to the total spin-only value; an ordered structure intermediate to *B*-6-2 and *B*-4-4 should give rise to a diffraction pattern exhibiting superlattice lines, the intensities of which depend upon the square of the difference of the magnetic scattering amplitude of Mn^{+3} and Mn^{+4}. These superlattice reflections will always be weak but in favorable cases should be just observable. No such superlattice lines were found and this suggests that the system is not completely ordered. A disordered arrangement of Mn^{+3} and Mn^{+4} ions over the lattice sites is consistent with the resistance minimum[14] observed near $x=0.3$ and with the fact that for these compositions the structure is nearly cubic.[11]

The sharp decline of the ferromagnetic moment as $x\rightarrow 0.5$ suggests that there is a strong tendency for antiferromagnetic coupling beyond this region. This trend can be reasonably accounted for on the bases (a) that beyond $x=0.5$ Mn^{+4}-O-Mn^{+4} antiferromagnetic bonds develop (b) the lattice spacings for $x>0.5$ are less than or equal to the spacing in the *A* type structure which is associated with a Mn^{+3}-O-Mn^{+3} antiferromagnetic bond, and (c) the antiferromagnetic *C-E* type structure which satisfies very well the over-all coupling requirements for $x=0.5$ is known to develop at nearly this composition.

Antiferromagnetic Region $x>0.5$

The various possible ordered arrangements of manganese ions in antiferromagnetic structures exhibited in Fig. 18 were postulated for the most part on the basis of the exchanges (a), (b), and (c) suggested in the first part of this section.

The structure type *A*-4-4 would be consistent with these exchange criteria if the Mn^{+3}-O-Mn^{+4} ferromagnetic exchange remained strong at this concentration. The fact that this structure is not observed for the $x=0.5$ composition may be due to other arrangements with fewer ferromagnetic bonds being more stable. For example the *C*-4-4 structure would also satisfy the requirements of the above exchange assumptions but

[14] J. H. Van Santen and G. H. Jonker, Physica **16**, 599 (1950).

this also was not observed. The *C-E* structure however, is a satisfactory and interesting occupant of the 50% Mn^{+4} region. On the basis of the previous assumptions of the coupling between Mn^{+3} and Mn^{+4} ions the ordering would be a combination of the elements *C*-4-4, *E*-6-2, and *E*-2-6. It is this type of ordering which gives the intensities shown in the second column of Table II, which we have seen can be improved by the alternative ordering scheme, shown as the *C-E* arrangement in the inset of Fig. 18. This arrangement which calls for both ferro- and antiferromagnetic coupling in the Mn^{+4}-O-Mn^{+3} bond is in perfect accord with the semicovalent coupling criteria of Goodenough. The arrowheads in the diagram of this structure have been incorporated to bring out in a simple way some of the elements of the theory. Each arrow represents essentially the overlap of a hydridized manganese ion orbital with a neighboring oxygen *p* orbital. According to the theory overlap on both sides of the intervening oxygen ion gives antiferromagnetic coupling whereas overlap on only one side leads to ferromagnetic coupling. In the figure which is meant only to be suggestive of the ideas involved, Mn^{+4} ions are represented as having octohedral orbitals and Mn^{+3} ions as having square coplanar orbitals, wherever this is consistent with the coupling criteria. The details are given in the following paper.

With increasing Mn^{+4} content for $x>0.5$, the magnetic structure changes from the *C-E* type to the *C* type which is found at concentrations near $x=0.75$. No ideal ordering scheme for the *C*-type has been found but an arrangement can be built up of units such as that illustrated under *C*-2-6 in which one-third of the Mn^{+4} ions are mismatched with respect to the preferred antiferromagnetic coupling. It must be emphasized, however, that the *C*-2-6 entry is not now an octant of the unit cell but it is included to illustrate the type of ordering suggested.

For ion concentrations near $x=1$ the *G* type structure is stable. This structure can be considered as consisting of two interpenetrating antiferromagnetically coupled lattices. For $CaMnO_3$ samples with some admixture of Mn^{+3} ions the data (see Sec. 13) were found to be consistent with the hypothesis that the net moment of each lattice is reduced because the Mn^{+3} ions enter the lattice with opposite spin to the Mn^{+4} ions which they replace, and hence it can be concluded that in this region also the Mn^{+3}-O-Mn^{+4} exchange is ferromagnetic.

It has been found that the set of magnetic structures and transitions which have been deduced from the experimental data on this series of compounds are in most respects consistent with the simple empirical rules (a), (b), and (c) regarding the types of indirect coupling between the manganese ions in these compounds. A basis for the types of compounds encountered in this problem and consequences thereof is given by Goodenough in terms of a semicovalent theory of exchange in the following paper wherein some discussion will be found also on the relation of the superexchange mechanism of Kramers[15] and Anderson[16] and of the double exchange of Zener[17] to these perovskite-type compounds.

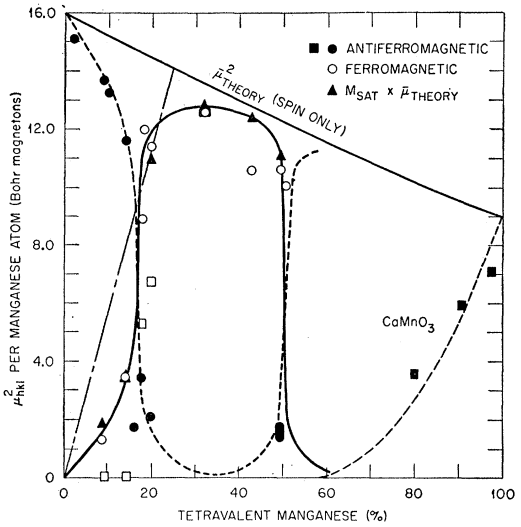

FIG. 19. Ferromagnetic and antiferromagnetic moments as a function of sample ion composition.

13. FERROMAGNETIC AND ANTIFERROMAGNETIC MOMENTS *VERSUS* COMPOSITION

The magnetic moment data which have been obtained in this investigation are summarized in Table I and are presented graphically as a function of sample composition in Fig. 19. For the discussion of this figure it will be necessary to show the relation of the plotted quantities to the experimental data.

In the neutron diffraction experiments the measured quantities are the absolute values of the integrated power in the various magnetic reflections. From the power in a given peak and the known parameters one obtains the quantities which for all the cases to be considered here[18] can be represented as $q^2jF_{hkl}^2$ where j is the multiplicity of the set of planes (hkl) and $q^2=1-(\mathbf{e}\cdot\mathbf{k})^2$ where $\mathbf{e}$ is the unit scattering vector and $\mathbf{k}$ is a unit vector in the direction of alignment of the ionic magnetic moments. For some structures, e.g., *B* and *G*, $q^2=\frac{2}{3}$ for all reflections and hence one can obtain no information about the moment orientation in the lattice. For other structures, such as Type *A*, the intensities in the pattern depend upon the moment orientation relative to the crystalline axes and therefore in such cases information relative to the moment orientation can be obtained. When q^2 has been evaluated for a given magnetic system one can obtain the quantity μ_{hkl} which is defined in terms of the measured

[15] H. A. Kramers, Physica **1**, 182 (1933).
[16] P. W. Anderson, Phys. Rev. **79**, 350 (1950); **79**, 705 (1950).
[17] C. Zener, Phys. Rev. **82**, 403 (1951).
[18] In common antiferromagnetic lattices where there are only parallel and antiparallel spin orientations q^2 can be represented as shown for unpolarized neutrons whereas in the more general case the vector $\mathbf{q}=\mathbf{e}-(\mathbf{e}\cdot\mathbf{k})\mathbf{k}$ must be appropriately introduced under the summation sign in Eq. (1).

quantity $|F_{hkl}|^2$ as

$$\mu_{hkl}=\frac{|F_{hkl}|}{n(e^2\gamma/2mc^2)f(\theta)}=\frac{1}{n}\left|\sum_n \mu_n e^{i\varphi_n} e^{2\pi i(hx_n+ky_n+lz_n)}\right|, \quad (1)$$

where γ is the neutron magnetic moment, $f(\theta)$ is the form factor of the magnetic electrons and is assumed here to be the same for all the ions in the system, μ_n is the magnitude of the ionic moment and $\varphi_n=0$ or π for orientations parallel or antiparallel to the direction of alignment of the spin system. The sum is to be taken over the n atoms of a unit cell. For a system which has some degree of randomness in the location of the moments on the lattice sites proper account must be taken of the randomness in applying Eq. (1) to the observations.

The values of μ_{hkl} obtained from the measured intensities may involve the individual ionic moments in different ways depending upon the structure and upon the particular reflection (hkl) considered. In succeeding paragraphs the measured quantities μ_{hkl}^2 are interpreted in terms of the individual ionic moments for a number of cases experimentally encountered and these are the quantities which are plotted in the figure and entered in the table. This representation has been adopted to represent on a single plot as much of the magnetic data as possible although this is not entirely satisfactory for all aspects of the problem.

For the pure A and G type structures where there is only one kind of magnetic ion, the value of μ_{hkl} as obtained from the observed F_{hkl} yields the magnetic moment per Mn^{+3} or Mn^{+4} ion respectively. It is seen that for the purest $LaMnO_3$ sample ($Mn^{+4}\sim 2\%$) the point on the graph is in good agreement with the expected value. The $CaMnO_3$ case will be considered later.

For the magnetic structure involving mixed Mn^{+3} and Mn^{+4} compositions an evaluation of the ionic moments requires in general a determination of the type of ionic ordering on the lattice sites. For the ferromagnetic cells opposite B in Fig. 18 the reflections with all indices even give $\mu_{hkl}=p_3\mu_3+p_4\mu_4$ where p_3 and p_4 are the fractional Mn^{+3} and Mn^{+4} contents, respectively, and μ_3 and μ_4 refer to the magnitudes of the moments of trivalent and tetravalent ions, respectively. This is the same result that one would obtain for a random distribution of Mn^{+3} and Mn^{+4} ions over the lattice sites. Depending upon the particular ordering scheme there will also be reflections other than those with all even indices which will yield the difference of the moments $(\mu_3-\mu_4)$. A discussion of the ordering in the ferromagnetic region was given in the last section. In any case $\bar{\mu}_F=p_3\mu_3+p_4\mu_4$ is the weighted average moment per ion in the ferromagnetic lattice and it is the square of this quantity, as determined from the neutron intensities which is plotted in Fig. 19 and listed in Table I.

In the mixed phase region ($0<x<0.25$) the measured values of $q^2jF_{hkl}^2$ for the two types of phases A and B should be proportional to $p_A\bar{\mu}_A^2$ and $p_F\bar{\mu}_F^2$, respectively, in which p_A is that fraction of the atoms in the sample which are associated with long-range antiferromagnetic ordering and p_F is the corresponding fraction for long-range ferromagnetic ordering. The average moment per ion in the ferromagnetic phase denoted by $\bar{\mu}_F$ has the definition given above. The average moment per ion in the antiferromagnetic phase $\bar{\mu}_A$ would be μ_3 if all the available Mn^{+4} ions tended to cluster in the ferromagnetic phase or would be $p_3\mu_3+p_4\mu_4$ if a fraction p_4 of the ions in the antiferromagnetic phase were tetravalent.

In the figure the effective squared moments $p_F\bar{\mu}_F^2$ and $p_A\bar{\mu}_A^2$ have been plotted as a function of ion concentration. It is evident from the figure that the growth of the effective ferromagnetic moment with increasing Mn^{+4} content in the low Mn^{+4} percentage region is less rapid than the line from 0 to $x=0.25$ which represents the maximum rate of formation of B-6-2 type ferromagnetic cells. It is not unreasonable to expect that for very small concentrations of Mn^{+4} a modified A-type structure would develop and that moderately high concentrations would be necessary for the cooperative coupling of Mn^{+3}-O-Mn^{+4} ions to produce long range ferromagnetic order. The long-range ferromagnetic order is seen to develop very rapidly near $x=0.15$, approaches full development in the vicinity of $x=0.25$ and remains large until x approaches 0.5. These results tend to lend support to the proposed ionic ordering schemes B-6-2 and B-4-4.

Information on the ferromagnetic moments, which has so far been discussed in this section in terms of the neutron measurements only, can also be obtained from direct magnetic saturation measurements (see Sec. 9). In the case of incoherent mixtures of ferro- and antiferromagnetic phases one would expect the observed saturation moment per magnetic ion in the sample to be given by $\bar{\mu}_{sat}=p_F\bar{\mu}_F$ where as previously p_F represents the fraction of the magnetic ions which are ferromagnetically aligned with an average moment $\bar{\mu}_F$. Comparison of these measurements with those obtained from neutron diffraction, which gives $p_F\bar{\mu}_F^2$, is conveniently done by plotting in Fig. 19 the quantity $\bar{\mu}_{sat}\times\bar{\mu}_F=p_F\bar{\mu}_F^2$ where the multiplying factor $\bar{\mu}_F$ is taken as the spin only value appropriate to the particular Mn^{+4} concentration. These data are represented by the triangles in Fig. 19, and it is seen that they agree quite closely with open circles from neutron diffraction measurements.

The validity of the above comparison and the apparent agreement between the neutron and saturation moment data depends on the criteria used to determine the ferromagnetic scattering from the neutron pattern. It was seen in connection with the discussion of Fig. 9 that measurements (a) above and below the Curie point and (b) with and without a magnetic field, gave essentially the same ferromagnetic scattering value in the first two reflections [but not

for the strong (222) reflection] and the moment corresponding to these two reflections agrees with that obtained from the magnetic saturation measurements.

In the case of the ferro- and antiferromagnetic mixed phases there is, however, some ambiguity in the interpretation of the ferromagnetic moments. It was shown in Fig. 10 that a magnetic field of about 4500 oersteds did not obliterate the (200) reflection and in fact for samples with low ($<14\%$)Mn^{+4} content no change in the (200) intensity was produced by the applied field. The moments determined by the field effects on the (200) reflections are represented in Fig. 19 by the squares.

If on the other hand the ferromagnetic moments are given by the total integrated intensity of the (200) temperature difference reflections one obtains the values plotted as open circles in Fig. 19. These values are seen to agree well with the corresponding ferromagnetic saturation measurements represented by the triangles in the figure.

In determining the trend of the ferromagnetic moment data the solid line was drawn through the $\bar{\mu}_F^2$ data obtained from the temperature difference curves, because it was felt that the agreement of these data with the ferromagnetic saturation measurements was strong evidence for identifying the (200) temperature difference peaks with the coherent magnetic scattering even if their intensities could not be effected by a magnetic field. The lack of field sensitivity for the coherent reflections and not for the usual saturation measurements is a point for which we have no satisfactory explanation at this time. The nature of the magnetization and hysteresis curves for the $LaMnO_3$ No. 65 sample for which the neutron magnetic field effect is negligible will also need further study before it can be satisfactorily accounted for.

For the *C-E* type structure observed at a Mn^{+4} content of about 58% the values of μ_{hkl}^2 obtained from the data can, as has been described, lead to an estimate of the moments occupying the several types of lattice sites. For the ordering shown in Fig. 18 and for the ideal composition, there will be two values of μ_{hkl}^2, of which one is proportional to μ_3^2 the other to μ_4^2. The departure of the sample from the ideal stoichiometric composition was shown to introduce modifications in the intensity pattern which could be accounted for if the excess Mn^{+4} ions were introduced into the Mn^{+3} sites at random but with reversed spin. In this case the observed μ_{hkl}^2 for the Mn^{+3} sites can be said to be proportional to $\bar{\mu}_3^2$ where $\bar{\mu}_3 = p_3\mu_3 - p_4\mu_4$ and is the weighted average, taking into account the spin reversal, of the moments of the ions on the ideal Mn^{+3} sites. For this case one cannot define an average magnetic moment in the sense described above and hence no entry is made in the figure.

In the case of the *C* type pattern, the μ_{hkl} values for reflections 110, 112, 130, etc., will all be proportional to $p_3\mu_3 + p_4\mu_4 = \bar{\mu}_A$ irrespective of the type of ordering provided that where there are misfits there are no spin inversions. That this seems to be the case is indicated by the fair agreement of the observed $\bar{\mu}$ value with that expected from the above model (2.99 observed *vs* 3.20 calculated). The observed value is however somewhat lower than expected and may represent an incomplete development of the structure. Accordingly for this case also no entry has been made in the figure.

The suggested growth of antiferromagnetic phases in the region $x>0.5$ is indicated by a rising and leveling off of the antiferromagnetic moment curve in this region.

The *G* type structure is apparently stable for compositions with $x>0.8$. For this structure only reflections which have all indices odd are permitted and for them $\mu_{hkl} = p_4\mu_4 \pm p_3\mu_3 = \bar{\mu}_A$. The + sign is to be taken if the Mn^{+3} ion in compositions different from $x=1$ replace Mn^{+4} with the same spin and the negative sign if they go into the lattice with spin opposite to the replaced Mn^{+4} ions. The predicted curve for this latter case is shown in the figure and it seems to agree well with the observed points. For the first case the average moments would have increased with Mn^{+3} content.

14. ACKNOWLEDGMENTS

The authors gratefully acknowledge the assistance received from their colleagues in the laboratory. They are indebted to Mr. R. H. Ward for assistance in the design of the spectrometer, to Mr. D. E. LaValle for assistance with sample preparations, to Mr. A. D. Horton for the chemical analyses and to Dr. H. L. Yakel for his x-ray studies and permission to use his data prior to publication. Helpful conversations and correspondence with Dr. John B. Goodenough of Lincoln Laboratories regarding the theoretical aspects of the problem are also gratefully acknowledged.

Note added in proof.—Additional data on the temperature dependence of lattice constants similar to that shown in Fig. 17 has recently been obtained by Yakel. These data concern the nearly ionically pure sample of $LaMnO_3$ No. 12 which shows the large lattice distortion at room temperature and below. The new data taken at elevated temperatures show a slow gradual decrease in splitting up to about 400°C after which there is a much more rapid decrease until at about 485°C the apparent symmetry becomes cubic. This constitutes a further illustration of the ordering transformation in the directed orbitals proposed by Goodenough for these compounds. We wish to thank Dr. H. L. Yakel for permission to quote these results.